Trident: Interference Avoidance in Multi-Reader Backscatter Network via Frequency-Space Division

Yang Zou, *Student Member, IEEE*, Xin Na, *Student Member, IEEE*, Yimiao Sun, *Student Member, IEEE*, and Yuan He, *Senior Member, IEEE, Member, ACM*

***Abstract*— Backscatter is a key technology for battery-free sensing in industrial IoT applications. To fully cover numerous tags in the deployment area, one often needs to deploy multiple readers, each of which communicates with tags within its communication range. However, the actual backscattered signals from a tag are likely to reach a reader outside its communication range and cause interference. Conventional TDMA or CSMA based approaches for interference avoidance separate readers' media access in time, leading to limited network throughput. In this paper, we propose Trident, a novel backscatter design that enables interference avoidance via frequency-space division. By incorporating a tunable bandpass filter and multiple terminal loads, a Trident tag can detect its channel condition and adaptively adjust the frequency and the power of its backscattered signals. We further propose a frequency assignment algorithm for the readers. With these designs, all the readers in the network can operate concurrently without being interfered. We implement Trident and evaluate its performance under various settings. The results demonstrate that Trident enhances the network throughput by 3.18×, compared to the TDMA-based scheme.**

***Index Terms*— Backscatter network, interference avoidance, multi-reader backscatter, low-power hardware design.**

I. Introduction

BACKSCATTER is an enabling technology for battery-free sensing applications in the industrial Internet of Things (IoT) [1], [2], [3], [4], [5], [6], [7], [8], [9], [10], [11]. Deploying a backscatter network in large factories requires dense deployment of readers for full backscatter coverage of the deployment area. In an ideal scenario, each reader covers a small area, enabling excitation and communication with tags in the vicinity. In reality, however, the backscattered signals from a tag are likely to reach a reader which the tag is not intended to communicate with [12], inducing undesired interference and potentially degrading the network throughput, as shown in Fig. 1.

Conventional approaches to deal with the above interference issue in a backscatter network are either TDMA-based or CSMA-based. In TDMA-based approaches, the readers, need to be carefully coordinated so that adjacent readers do not excite a tag simultaneously [13], [14], [15]. This coordination, whether distributed or centralized, introduces significant complexity and cost in communication. In CSMA-based schemes, a reader needs to take back-offs when the channel is occupied by another reader, and can't send out the excitation until the channel is clear [16]. Both TDMA or CSMA based schemes can avoid interference, however, at the cost of network throughput. This is because they sorely focus on the readers and avoid interference only in the time domain.

In this paper, we consider a novel interference avoidance method, which utilizes other multiplexing spaces to tackle the interference problem and in turn to improve the overall throughput of the backscatter network. To achieve this, we propose to empower the backscatter tags with the ability to avoid interference in the frequency and space domains. The backscatter network operates at multiple frequency bands. Adjacent readers are assigned to work at different bands. A tag detects its channel condition and adaptively determines a reader to communicate with. To avoid interference to the readers, the tag should be able to select the frequency band with the strongest excitation signal and only backscatter signals at that band. The power of the backscattered signal should also be finely controlled to avoid interference with another remote reader that works at the same band.

Implementing the above idea is a daunting task, which may meet the following critical challenges:

1) Given the highly limited power budget of battery-free tags, typically less than 1mW [17], a significant challenge arises in realizing the aforementioned innovative capabilities involving band selection and frequency-selective reflection.
2) Selective reflection is a missing piece in the state of the arts. In the existing works, a tag usually backscatters signals across the whole frequency range. How to generate backscattered signals in only one of the multiple bands is a hard problem, especially considering the limited process capacity of a tag.
3) For the purpose of space division, the power of the backscattered signals should be finely controlled, but how to ensure the efficacy of power control under dynamic channel conditions remains a challenging issue.

In this paper, we present **Trident**, a novel backscatter tag to tackle the aforementioned challenges. A Trident tag contains a **frequency band detector**, which utilizes a frequency-tunable

Received 6 January 2024; revised 30 August 2024; accepted 21 October 2024; approved by IEEE/ACM TRANSACTIONS ON NETWORKING Editor S. M. Kim. This work was supported by the National Natural Science Foundation of China under Grant 62425207 and Grant U21B2007. *(Corresponding author: Yuan He.)*

The authors are with the School of Software & BNRist, Tsinghua University, Beijing 100084, China (e-mail: zouy23@mails.tsinghua.edu.cn; xn20@mails.tsinghua.edu.cn; sym21@mails.tsinghua.edu.cn; heyuan@tsinghua.edu.cn).

Digital Object Identifier 10.1109/TNET.2024.3495660

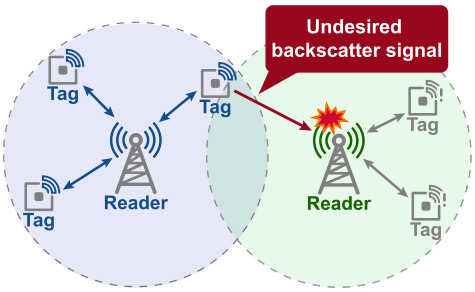

Fig. 1. Illustration of interference in the multi-reader backscatter network.

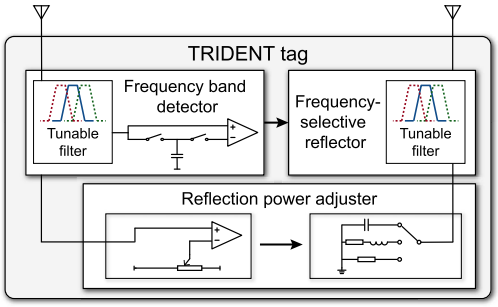

Fig. 2. The three key components of Trident tag.

bandpass filter to extract signals from different bands and a low-power two-step comparator for signal strength comparison. We exploit the characteristics of bandpass filters in signal reflection and propose a new scheme for **frequency-selective reflector**. We further develop a **reflection power adjuster**, which selects suitable terminal loads for the reflector to control the backscattered signal strength, so that the interference range of the tag doesn't cover the other readers. To facilitate the Trident's deployment in multi-reader environments, we propose a frequency assignment algorithm, ensuring adjacent readers operate on different bands. Including the above designs, Trident realizes frequency-space division in a backscatter network and significantly enhances the efficiency of interference avoidance.

Our contributions can be summarized as follows:

- Trident is the first-of-its-kind work that empowers a backscatter tag with the ability of band detection and frequency-selective reflection in the sub-6G band.
- We propose a reflection power adjustment scheme based on excessive power detection and terminal load selection, which controls the strength of backscattered signals and avoids interfering the same-band readers via space division.
- We introduce a frequency assignment algorithm, which assigns frequencies to readers in complex multi-reader deployment, avoiding co-frequency interference among adjacent readers.
- We implement Trident tag on a printed circuit board (PCB) and deploy a multi-reader backscatter network prototype. The results show that Trident enhances the network throughput by 3.18×, compared to the TDMA-based scheme.

The remainder of this paper is structured as follows. We elaborate on our tag design in Section II and the frequency assignment algorithm in Section III. Then we introduce some practical issues in Section IV and the system implementation in Section V. Section VI presents the evaluation results. Section VII reviews the related works. We conclude this paper in Section VIII.

II. Trident Tag Design

A. Overview

In this section, we propose the design details of Trident tag, as shown in Fig. 2. Trident tag mainly consists of three essential components:

Frequency band detector: The frequency band detector accomplishes band detection through two steps: extracting excitation signals at various frequency bands and comparing the strengths pairwise. To extract signals at various bands, we explore a frequency-tunable bandpass filter model that demonstrates the relationship between the center frequency and resonant capacitance, then we implement this filter using varactor diodes. For strength comparison, we notice the signal strength can be converted into voltage by an envelope detector and stored in a capacitor. Thus we utilize the tunable filter to sequentially extract signals from two bands, storing the detection voltage of the previous one and comparing it with the next one. This approach enables low-power strength comparison.

Frequency-selective reflector: We achieve generating signals only at a specific band by greatly attenuating backscattered signals out of this band. For the methodology of generating backscattered signals with different strengths in various bands, we investigate the mathematical model of backscattered signals and identify that the variation of the reflection coefficient determines the backscattered signal strength. Then we find that the bandpass filter's reflection coefficients for signals outside the passband are nearly constant. And based on the filter we develop a frequency-selective reflector.

Reflection power adjuster: When the excitation signal is strong, the reflected signal tends to be strong and can cause interference to distant readers operating at the same frequency. To finely control the strength of the backscattered signal, we introduce a detector to detect excessively strong excitation signals based on a threshold voltage comparator. Then, building upon the understanding that variations in the reflection coefficient directly impact the strength of backscattered signals, we explore the relationship between the reflection coefficient and the impedance of terminal loads. We design multiple selectable terminal loads that enable adjustment over the backscattered signal strength. Thus we build a reflection power adjuster, enabling adaptively control of the reflection strength.

Next, we will introduce the frequency band detector and the frequency-selective reflector, followed by the design of the reflection power adjuster.

B. Frequency Band Detector

1) Signal Extraction: The first step in detecting the frequency band with the strongest excitation is to extract excitation signals at each individual band. To accomplish this

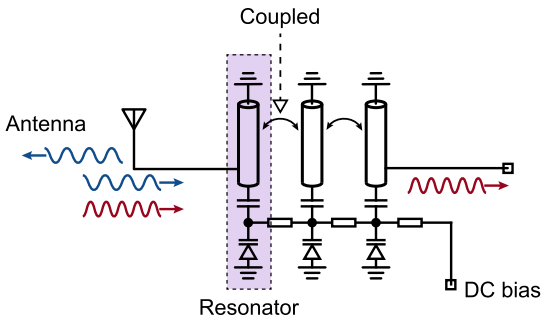

Fig. 3. The structure of the frequency-tunable bandpass filter.

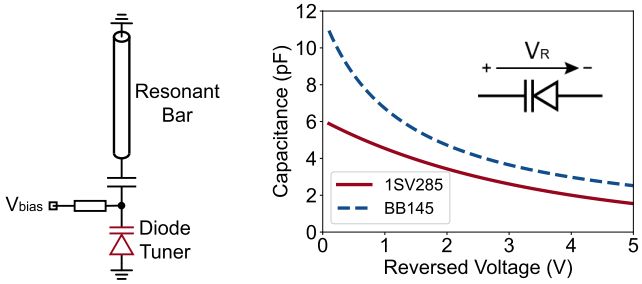

(a) The structure of the resonator.

(b) The capacitance-voltage curve of the varactor.

Fig. 4. Trident tag adjusts the V_{bias} of the varactor diode to change its capacitance, thus tuning the resonator.

objective while minimizing power consumption, we incorporat a frequency-tunable bandpass filter in the next stage of the antenna [18].

As shown in Fig. 3, the bandpass filter consists of three parallel coupled tunable resonators, and each resonator has a specific resonant frequency f.

f is determined by the two components of the resonator: a resonant bar and a resonant capacitor, according to:

$$L = \frac{Z_0 \tan(2\pi f l/v)}{2\pi f} \tag{1}$$

$$f = \frac{1}{2\pi\sqrt{LC}} = \frac{1}{2\pi Z_0 \tan(2\pi f l/v) C} \tag{2}$$

where C represents the capacitance value of the resonant capacitor. v, Z_0 and l correspond to the speed of electromagnetic waves, characteristic impedance, and length of the resonant bars, respectively.

The equation above indicates that we can change the resonant frequency by varying the resonant capacitor, thereby tuning the filter's center frequency. Thus we consider using varactors as the resonant capacitors in our tunable filter design. The varactor typically operates in a reverse-biased state, and its capacitance depends on the reversed voltage, according to:

$$C = \frac{C_0}{(1 - V/V_0)^\gamma} \tag{3}$$

where C_0 is the junction capacitance with no bias. V_0 and γ depend on the diode type and are constants for a specific diode. Specifically in Fig. 4(b), we show the junction capacitance versus the voltage for diode 1SV285 [19] and BB145 [20]. By using the varactor, we can adjust the resonant capacitance value by providing a set of different bias voltages, further tuning the center frequency of the bandpass filter among several bands. Furthermore, the varactors only consume a current of several nAs, introducing negligible additional power consumption to the tag.

To provide different bias voltages to the tunable bandpass filter, a resistor voltage divider circuit is employed. This circuit utilizes an SPNT (i.e., single-pole N-throw) analog switch to connect various resistances to the voltage divider circuit. By manipulating the analog switch, the voltage divider circuit generates different bias voltages, thereby facilitating the adjustment of the filter's center frequency.

The frequency-tunable bandpass filter is employed in the next stage of the antenna. When the frequency of the input signal deviates significantly from the resonant frequency, the resonators fail to resonate, resulting in weak electromagnetic oscillation. Consequently, the input excitation signal is unable to traverse to the terminal through the coupling and instead gets reflected back by the filter.

When the frequency of the input RF signal matches the resonant frequency, the amplitude of the electromagnetic field oscillation around the resonator is significant. This allows the signal to be coupled and transmitted to the adjacent resonator, even if the two resonators are not directly connected. Through successive coupling, the signal propagates and eventually passes through the entire filter. Thus the signal in a specific frequency band is extracted.

2) Two-Step Strength Comparison: After the signal extraction, we use an envelope detector to convert the strength of the excitation signal at that band into a voltage output. By comparing the output voltages across the different frequency bands, the tag can identify the band with the strongest excitation signals.

Instead of employing ADC to sample the output voltages and comparing them with each other, which would augment tag complexity and lead to increased energy consumption, we propose a method in which the output voltages are stored in capacitors before being compared. This approach avoids the need for directly obtaining accurate voltage values, and by using pairwise comparisons, the tag can identify the frequency band with the strongest excitation signal.

Our frequency band detector performs a comparison of the excitation signal strength in two frequency bands in two steps, as illustrated in Fig. 5. Firstly, the center frequency of the tunable bandpass filter is adjusted to *Band 1*, and then switch S1 is closed while switch S2 is open. At this stage, the envelope detector converts the excitation signal strength in *Band 1* into voltage V_{band1}, and the capacitor is charged to V_{band1}. Next, the center frequency of the tunable bandpass filter is adjusted to *Band 2*, and S1 is opened while S2 is closed. Now the inputs of the comparator are the voltage V_{band1} stored in the capacitor, representing the signal strength of *Band 1*, and the voltage V_{band2} outputted by the envelope detector, representing the signal strength of *Band 2*. The output level of the comparator indicates the result of the comparison between the signal strength of the two bands: if the output level is high, it means *Band 2* has a stronger signal, otherwise, *Band*

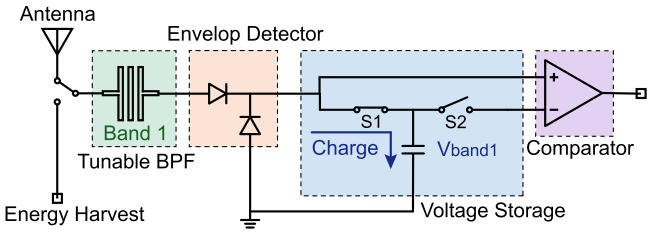

(a) *Step1:* Charge.

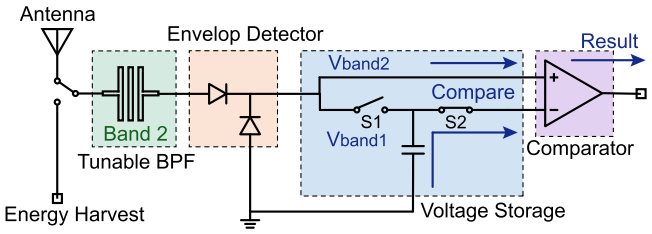

(b) *Step2:* Compare.

Fig. 5. The frequency band detector completes the comparison of signal strengths at two frequency bands through two steps.

1 has a stronger signal. By performing two comparisons, this circuit can determine the frequency band with the strongest excitation signal among the three frequency bands.

Besides, the capacitor could experience slight voltage reduction due to the leakage current of the comparator and analog switches. This leads to potential inaccuracies in the voltage comparison, especially when the two voltages are very close. Thus, The tag will exchange the order of two voltage inputs and then perform another comparison. If the result of the two comparisons differs, the tag will consider the signal strengths in those two frequency bands to be practically the same and randomly choose one as the comparison result.

C. Frequency-Selective Reflector

We consider the frequency-selective reflection as the capability of generating a strong backscattered signal only at a specific frequency band while producing weak signals in other frequency bands. For the methodology of generating reflection signals of different strengths in different frequency bands, we first analyze the mathematical model of the backscattered signal and study the factors that influence the strength of the backscattered signal.

When the tag controls the RF switch to toggle between two terminal loads. The signal received by the reader can be represented as:

$$y(t) = \alpha x(t) + \beta B(t) x(t) + n(t) \tag{4}$$

where $x(t)$ is the reader's excitation signal, $n(t)$ is the noise, α and β are the complex attenuation of the excitation signal and the backscattered signal, and the $B(t)$ are either Γ_1 or Γ_2, which are complex reflection coefficients corresponding to the two terminal loads. The average of the second term, $\beta(\Gamma_1+\Gamma_2)x(t)/2$, corresponds to the unchanged reflection of the excitation signal and does not carry any tag information. Thus when calculating the strength of the backscattered signal, this part should be subtracted, and the strength should be written as $|\beta(\Gamma_1-\Gamma_2)x(t)/2|$. This implies that the strength of

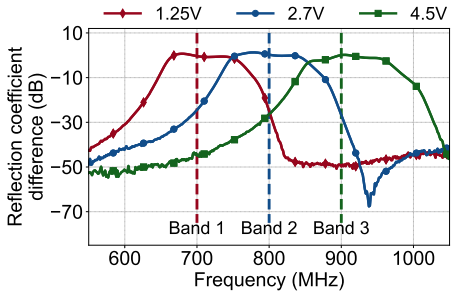

Fig. 6. The operating frequency band of the reflector changes with the variation of the bias voltage.

the backscattered signal depends on the difference in reflection coefficient when the tag switches its terminal loads. Therefore, if we ensure that the reflector exhibits a significant variation of reflection coefficient only at one frequency band, we can achieve the frequency-selective reflection.

According to the characteristic of the tunable bandpass filter described in the previous part, when the input signal frequency matches the center frequency of the filter, the signal can reach the switchable terminal loads, thus the reflection coefficient of the entire reflector for that frequency signal is primarily determined by the impedance of the terminal loads. For signals with frequencies different from the filter's center frequency, they are directly reflected back by the filter, thus the reflection coefficient of the reflector for that frequency signal is determined by the filter and remains unchanged when terminal loads are switched.

Based on the above analysis, we consider adding a voltage-tunable bandpass filter mentioned above in front of the traditional RF switch to form a frequency-selective reflector. To confirm the feasibility of this approach, we measure the difference in reflection coefficients in various frequency bands when the reflector toggles the terminal loads. Fig. 6 illustrates the difference in reflection coefficients for two different terminal loads corresponding to three different bias voltage inputs applied to the reflector. Although the reflection coefficient difference of the reflector under three bias voltage inputs may not be completely isolated from each other, each peak corresponds to only one frequency band, and the changes in reflection coefficient for the other two bands are minimal. This indicates that when the reflector selects a specific frequency band, it will generate a strong backscattered signal only at that band, while the backscattered signal in the other frequency bands is extremely weak. Hence, this reflector exhibits excellent capability of frequency-selective reflection.

D. Reflection Power Adjuster

In backscatter communication, the strength of backscattered signals is directly related to the strength of the excitation signal, which varies with the distance between the tag and the reader. In the case of a tag being close to a reader, its backscattered signal can be excessively strong and cause interference to distant readers operating at the same frequency. To control the strength of backscattered signals, the tag first needs to detect the strength of the excitation signal. Thus, we introduce the excessive power detector.

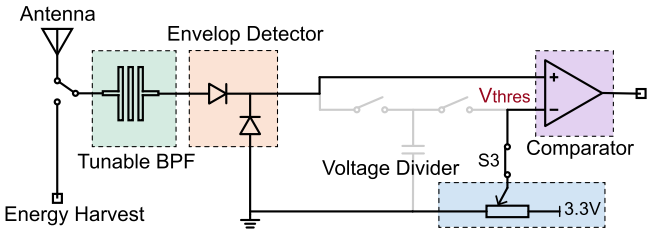

Fig. 7. The excessive power detection circuit design based on the frequency band detector.

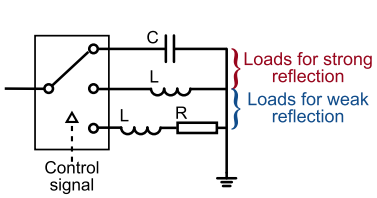

(a) The schematic of the multiple selectable impedances.

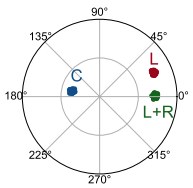

(b) The reflection coefficients of the impedances of L, C and series of L and R.

Fig. 8. The multiple impedance selection circuit and the reflection coefficients for each impedance.

Noticing that the envelope detector converts the strength of the excitation signal into a voltage output, allowing for checking whether the excitation signal is excessively intense through a threshold voltage comparison. Considering the frequency band detector already includes an envelope detector and voltage comparator, we add a threshold voltage comparison circuit to the frequency band selector to implement the excessive power detector, as shown in Fig. 7. This design can also help to simplify the tag design and reduce power consumption.

When S3 is closed, the threshold voltage comparison circuit is connected and the detector enters excessive power detection mode. At this point, the comparator's inputs are the threshold voltage from the voltage divider circuit and the detection voltage from the envelope detector. Using the link budget theory [21], we calculate that when the excitation signal is stronger than -20dBm, the tag can interfere with the adjacent readers. Thus, the threshold voltage is set to 1.6V, which is the output voltage of the envelope detector when the excitation is -20dBm [22]. Finally, by comparing the detected voltage with the threshold voltage, the tag determines whether the current excitation signal is too strong.

Once the excessive power detector detects the strength of the excitation signal, the tag needs to adaptively adjust the strength of the backscattered signal based on the detection result. According to the expression for the backscattered signal strength described in the previous subsection, we can adjust the strength of the reflected signal by varying the difference in the reflection coefficients of the reflector.

Within the selected frequency band of the reflector, the reflection coefficient Γ for the input signal primarily depends on the impedance of terminal loads, according to the following equation:

$$\Gamma = \frac{Z_0 - Z_L}{Z_0 + Z_L} \tag{5}$$

where Z_0 is the characteristic impedance which is commonly 50Ω, and Z_L is the complex impedance of the terminal load. This equation can also be used to calculate the terminal impedance given the required reflection coefficients. We employ multiple selectable terminal loads with proper impedance on the tag's reflector. We carefully adjust the value of the load impedance to maximize the differential reflection coefficient for the higher SNR. The loads we designed include an inductor, a capacitor, and a series of an inductor and a resistor, as shown in Fig. 8. By selecting appropriate loads based on the strength of the excitation signal, the backscattered signal's strength can be controlled effectively.

When the strength of the excitation signals does not exceed the threshold, the terminal loads are switched between the inductor and the capacitor. Due to the opposite imaginary part of the impedance of the inductor and the capacitor, the variation in the reflection coefficient is relatively significant when switching between these two loads. It helps strengthen the backscattered signal, improving the communication performance between the tag and the reader.

When the excessive power detector detects an excessively strong excitation signal, the tag's loads are switched between the inductor and the series of an inductor and resistor. Because of the small difference in impedance of these two terminal loads, the variation in the reflection coefficient during this switch is relatively smaller, thereby reducing the strength of the reflected signal. This helps avoid interference with distant readers operating in the same frequency band.

III. Reader Frequency Assignment

Trident is required to operate in a backscatter network where the adjacent readers work on different bands. In this section, we propose an algorithm to assign the readers' working frequency bands, separating the same-band readers to avoid interference.

In an ideal scenario, we can employ a hexagonal grid deployment similar to LTE base stations [23]. However, the deployment of readers is often constrained by various factors in real IoT environments. We turn to carefully assign the operation frequencies to readers for interference avoidance.

We model the aforementioned issue as a coloring problem in an undirected graph. We construct an interference graph. Each node in the graph represents a reader. If the interference strength between two readers exceeds a safety threshold, an undirected edge is established between the nodes representing these two readers. We aim to color the nodes using three colors, intending for adjacent nodes to have different colors. This requires the graph to be a tripartite graph. However, due to the uncertainty in reader positions and the wireless channel, we can't guarantee that the graph is tripartite. Consequently, there might not exist an allocation method that entirely avoids interference.

We shift our focus towards finding the assignment with the least co-channel interference, which is an NP-hard problem.

Algorithm 1 Reader Frequency Assignment with Genetic Algorithm

Input: M_{ij}: Interference strength between readers
Output: F: Reader frequency assignment strategy

1 Initialize interference graph's adjacency matrix: $G_{ij} = (M_{ij} > Thres)?M_{ij} : 0$;
2 Initialize population with random individuals (assignments): $P_0 = [F_0, F_1, \cdots, F_{M-1}]$;
3 $cnt \leftarrow 0$;
4 **do**
5 **for** F_i *in* P_{cnt} **do**
6 **foreach** *Reader* R_j **do**
7 Find same-band readers' index K;
8 $E_j \leftarrow \sum_{k \in K} G_{jk}$;
9 $Error_i \leftarrow \text{mean}(E_j) + \text{median}(E_j)$;
10 **end**
11 **end**
12 $P_{cnt} \leftarrow$ top 10% individuals of P_{cnt}, ascending sorted by $Error_i$;
13 $P_{cnt+1} \leftarrow$ mate, mutate, expansion (P_{cnt});
14 $cnt \leftarrow cnt + 1$;
15 **while** $cnt < C$;
16 $F \leftarrow F_i$ in P_C with minimum $Error_i$;

Traversing through all possible solutions leads to a complexity of $O(3^n)$, which is impractical. Therefore, we propose an optimization algorithm, as shown in Alg. 1. This algorithm takes the interference strength between readers as its input, with the frequency assigned to each reader as the optimization object, aiming to minimize the strength of co-frequency interference. Considering that frequency allocation is an optimization problem with discrete variables, we employed a genetic algorithm. The algorithm unfolds through the following steps:

1) First, we initialize the edge weight of graph G_{ij} as the interference strength between the corresponding readers at both ends (Line 1). Subsequently, we initialize the frequency assignment F_i as individuals in population P_0, where $i \in [0, M-1]$ (Line2).
2) For each assignment method F_i within the population, we compute the total interference energy received by each reader, represented as E_j, i.e., the node strength (Line 7-8). We then utilize the sum of the maximum value and the median of E_j as the error. This selection considers both local and global optimization simultaneously (Line 9).
3) We select the top 10% individuals with the lowest error and use mating, mutation, and population expansion methods to generate the next generation P_{cnt+1}. We proceed with the next round of evaluation until the iteration count reaches the preset limit (Line 12-14).
4) Finally we output the individual with minimum error in population P_C as the optimized reader frequency assignment strategy (Line 16).

This algorithm requires the interference strength between readers to construct the interference graph. We set a bootstrap phase, during which one reader sequentially transmits test signals and other readers listen to the channel and record interference strength. This phase takes an average of 2.3s when the algorithm runs in an AMD R7-4800H CPU and will not impact the subsequent readings.

To adapt to the dynamic channel, we introduce a reallocation mechanism. After the frequency allocation, each reader listens and detects the interference from other readers, which is denoted as $\vec{v_0}$. And they periodically detect and report the current interference strength, denoted as $\vec{v_i}$. When the normalized dot product of $\vec{v_0}$ and $\vec{v_i}$ is less than the threshold, we consider that the channel has changed and reallocate the frequencies.

IV. Practical Issue

We complete the design of Trident by articulating some practical issues of its applicability.

A. Bandpass Filter Design

We incorporate two frequency-tunable bandpass filters in Trident tag, each serving distinct purposes: one for extracting the excitation signal and the other for generating backscattered signals within specific frequency bands. However, when the Q value of the bandpass filter remains constant, increasing the out-of-band suppression inevitably leads to greater in-band losses. Higher losses within the passband significantly weaken tag communication performance, while lower out-of-band suppression increases the risk of interfering with other frequency bands.

We set an out-of-band suppression target of 20dB. Leveraging the ANSYS HFSS optimization, we aimed to minimize in-band losses while ensuring out-of-band suppression. Additionally, we tailored the optimization objectives for the frequency band detector and frequency-selective reflector to focus on the S_{21} and S_{11} parameters of the filters, respectively, catering to the distinct purposes of the two bandpass filters.

B. Envelope Detector Selection

In prior work, researchers utilize passive [24], [25] or active [26] envelope detectors for the tags. However, the active envelope detector often consumes several mWs, exceeding the power constraints of the backscatter tag. While the passive envelope detector can output detection voltage without additional power consumption, it suffers from lower sensitivity. As the frequency band detection step in Trident tag requires precise detection voltage output, the passive envelope detector is not suitable for our design.

Reviewing the band detector's design, we noticed that the envelope detector works for only tens of microseconds to complete the band detection, instead of requiring continuous operation as seen in ambient backscatter tags [4]. By setting the band detection frequency to once every 3 seconds, the envelope detector operates at less than a 1‰ duty cycle, resulting in an average power consumption of just a few μWs.

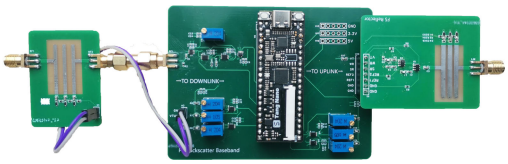

Fig. 9. Trident tag is implemented by commercial off-the-shelf components on PCB.

TABLE I
POWER CONSUMPTION OF TRIDENT TAG IMPLEMENTED IN 65NM CMOS TECHNOLOGY AND THE PCB PROTOTYPE

Part	Switches	Envelope detector	Control logic	
ASIC Power	3μW	7μW	2μW	
PCB Power	3μW	0.25mW	16.6mW	
Part	Comparator	Filter tuning	Clock	Total
ASIC Power	1μW	60nW	3μW	16μW
PCB Power	1.6mW	60nW	12mW	30.45mW

C. Capacitor Selection

In the frequency band detector, we utilize a capacitor to store the detection voltage. If the capacitance value is too small, leaked currents from switches and comparators can rapidly reduce its voltage, leading to erroneous signal strength comparison results. On the other hand, if the capacitance value is too large, the active envelope detector would need to operate for an extended period until the capacitor's voltage stabilizes, incurring higher power consumption.

We aim for the error between the capacitor voltage and the detector output voltage to be within 1%, after charging the capacitor for T_c seconds and considering leakage for T_l seconds. We can compute the upper and lower bounds of the capacitance value using classical circuit theory.:

$$C \leq C_{max} = \frac{T_c}{\ln(100)R_S} \quad C \geq C_{min} = \frac{100 I_l T_l}{V_{min}} \tag{6}$$

where R_s, I_l, and V_{min} are the output impedance of the envelope detector, the leak current of the CMOS switch, and the minimum valid output voltage of the envelope detector, respectively. We set T_c to 50 μs and adopt a capacitor of 10nF, which is the geometric mean of the capacitance values C_{max} and C_{min}. If we need to further reduce the energy consumption of the envelope detector, we can set a lower T_c and use a smaller capacitor.

V. IMPLEMENTATION

A. Trident Tag

We implement the Trident tag on PCB using commercial off-the-shelf components, as shown in Fig. 9. The tag consists of a frequency band detector with excessive power detection and a frequency-selective reflector with adjustable reflection strength.

In the frequency band detector circuit, the first component is the frequency-tunable bandpass filter. The filter is implemented using microstrip lines integrated on the PCB and three 1SV285 varactor diodes. To provide an adjustable bias voltage to adjust the center frequency of the filter, we use analog switches TS5A23166 to switch the resistors in the voltage divider circuit. For the two-step strength comparison circuit, we use the LT5534 envelope detector, which can effectively detect RF power above -40dBm. We control LT5534's EN pin to enable this chip only during the frequency band detection period for energy saving. The TS5A23166 analog switch is employed to toggle among the charging and two comparing modes (comparing with capacitor voltage or threshold voltage), and an NCS2200 low-power comparator is utilized for voltage comparison. This circuit enables the comparison of excitation signal strengths in two frequency bands and detects excessively strong excitation signals.

The reflector is composed of the tunable bandpass filter, the switchable terminal, and the control logic. The tunable bandpass filter is similar to that in the reflector. The switchable terminal utilizes two HMC544 RF switches to toggle among three terminal impedances, which can adjust the strength of the backscattered signals. Both the detector and the reflector are equipped with 3-dBi omnidirectional antennas.

The control logic is implemented using a low-power GW1NZ-1 FPGA. The FPGA utilizes square waves of different phases at a frequency of 1MHz to switch the terminal loads. This process generates a BPSK backscattered signal at the frequency band adjacent to the excitation signal at 1MHz to avoid self-interference.

The cost of making a PCB prototype is around $13. Compared to the existing backscatter tag designs, Trident's additional costs come from the varactor diodes in the tunable filter and the analog switch, which cost less than $1. Thus Trident is not expensive compared to the existing designs.

B. Reader

We implement the mono-static configured readers using the USRP N210 software-defined radio platform by Ettus Research. The USRPs are equipped with two 3-dBi co-located antennas separated by 30cm. The transmission antenna is connected to a UBX-40 daughterboard. To prevent excessive self-interference from damaging the RX chain, the reader transmission power is limited to +5 dBm. The receiving antenna is connected to the same daughterboard, which down-converts the received signals to the baseband and samples at a rate of 500 ksps. The reader can read tags within 1m. If we can cancel the self-interference in the RX chain like the commercial RFID readers, we could increase the transmission power and achieve a longer communication range.

C. Power Consumption

We evaluate the power consumption of an ASIC solution of the Trident tag [1], [31] and the PCB prototype. We report it in Tab.I. Trident with ASIC technology meets the energy constraints of backscatter tags with the power consumption of 16μW. The PCB prototype implementation has a power consumption of about 30mW. We also compare the power consumption and the energy efficiency of Trident and other backscatter technologies, which are enabled to avoid interference. We report it in Tab.II.

TABLE II
POWER CONSUMPTION AND ENERGY EFFICIENCY COMPARISON OF TRIDENT AND OTHER BACKSCATTER TECHNOLOGIES

Technology	Power consumption	Energy efficiency
OFDMA Backscatter [27]	18.31μW	0.079nJ/bit
NetScatter [28]	45.2μW	45.2nJ/bit
P2LoRa [29]	320 μW	28.39nJ/bit
mmComb [30]	87.3μW	1.59pJ/bit
Trident	16μW	0.16nJ/bit

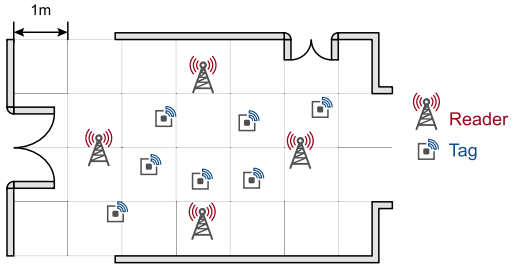

Fig. 10. Evaluation setting in a 4m×6m corridor.

VI. EVALUATION

A. Experimental Setup

We construct a Trident network prototype with 4 readers and 7 tags in an indoor corridor measuring 4m×6m. As shown in Fig. 10, the 4 readers were deployed around the center of the corridor and the 7 tags were randomly placed within the coverage area. The upper and lower readers in the figure operate at the same band, while the remaining two readers each use the remaining two bands, respectively. And when these tags detect the excitation signal, they would transmit a data packet of 128 bits at a rate of 100Kbps with a variable reporting rate from 100 packets per second(pps) to 500pps.

We present the overall evaluation results first. In the overall system evaluation, we take *overall throughput* as the key metric to assess the Trident network. *overall throughput* measures the average amount of backscattered data correctly decoded per second at all the readers in the network. Then we present our ablation study, where we evaluate the frequency selectivity, the accuracy of band selection, and the throughput increment by adjusting the reflection power. We also conduct simulation experiments to evaluate the frequency allocation algorithm.

B. Overall Throughput

We evaluate the overall throughput of the Trident network in terms of different tag numbers, reporting rates, reader density, and tag deployment. We construct a centralized TDMA network as the baseline and show Trident's performance gain. The CSMA network is not compared here since its media access efficiency is typically lower than TDMA [32]. Both networks use the same deployment plan of all the readers and tags to ensure that they are the same in terms of the SNR level.

1) Impact of Tag Numbers And Reporting Rate: We conduct four groups of experiments by varying the number of tags from 4 to 7. For each tag number setting, we vary the tags' reporting rate from 150pps to 400pps and measure the overall throughput. We have three observations based on the results shown in Fig.11.

First, we observe that Trident demonstrates a throughput improvement of 2.28-3.18× across various numbers of tags and reporting rate settings compared to the TDMA network. This is because readers do not need to operate intermittently in Trident, resulting in a three times increment in their operating time.

Second, we observe that the total throughput of Trident network increases linearly with the tags' reporting rate, while the throughput increase of the TDMA network gradually slows down. For instance, when the tag number is 6, for every 50pps increase in the reporting rate, the Trident network's throughput increases linearly by nearly 25Kbps. However, the throughput increment of the TDMA network decreases from 7.5Kbps to 3Kbps. The performance gain also increases with the reporting rate, ranging from 2.28-2.66× at a reporting rate of 150pps to 2.92-3.18× at a reporting rate of 400pps.

Third, when the reporting rate is high, the total throughput of Trident network continues to grow with the increasing tag number, while the increase in total throughput of the TDMA network is highly limited. At a reporting rate of 400pps, the average increase in throughput of the Trident network is 13.9Kbps per additional tag. (27.8% of the ideal throughput per tag). On the other hand, TDMA network only achieves an average increase of 7.7Kbps in throughput for each additional tag (15.4% of the ideal throughput per tag).

The reason is that a reader in the TDMA network can excite the tags which wouldn't respond to it in Trident network. This results in the reader communicating with more tags, and these tags cause more serious interference, especially under high reporting rate conditions. This evaluation demonstrates that Trident network performs better in scenarios where tag throughput is required to be high.

2) Impact of Readers' Density: We deploy 7 tags and set the reporting rate of each tag to 400pps. We set the distance between each pair of readers to 1.4m, 1.8m, and 2.2m to change the reader's density and measure the overall throughput in each setting.

The results are depicted in Fig. 12, as the distance between readers decreases, the throughput of Trident remains relatively constant at 230Kbps or even slightly increases. However, the throughput of the TDMA network decreases from 72Kbps to 69Kbps. From a performance gain perspective, the closer the distance between readers, the higher the gain of Trident. The performance gain increases from 3.18× at a reader distance of 2.2m to 3.33× at a distance of 1.4m. This is because the TDMA network activates more tags with higher reader density, leading to more severe tag-to-tag interference and adversely affecting the throughput. The result indicates that Trident is more suitable for environments with dense reader deployments than the TDMA network.

3) Impact of Tag's Deployment: We deploy 7 tags in the network, with each tag set to a reporting rate of 400pps. In addition to uniformly deploying tags throughout the entire experimental area, we deploy tags in the left half and front half of the area, creating two types of non-uniform tag

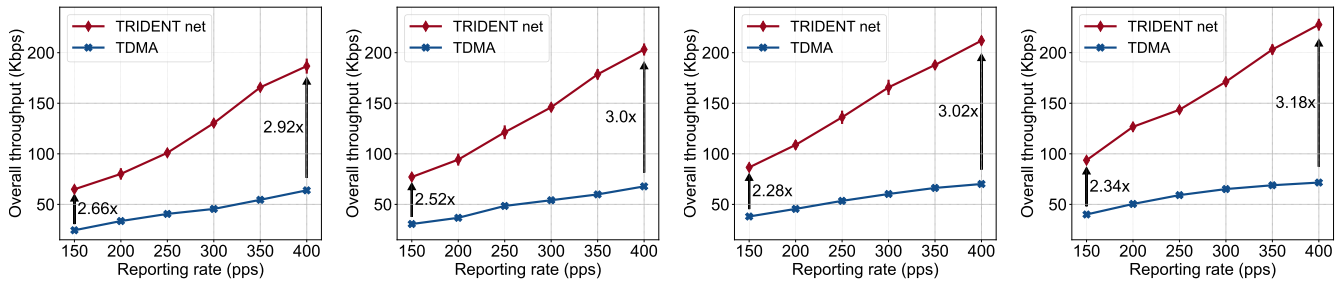

(a) Deploy 4 tags (b) Deploy 5 tags (c) Deploy 6 tags (d) Deploy 7 tags

Fig. 11. Overall throughput of Trident network and traditional TDMA network in different number of tags deployed in the network and reporting rate of each tag.

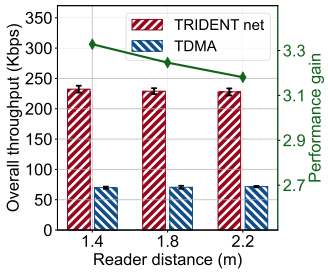

Fig. 12. Overall throughput comparison between two networks with reader density represented by the distance between readers.

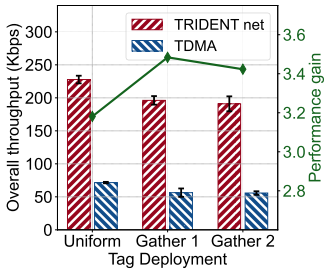

Fig. 13. Overall throughput comparison with three different tag deployment methods in the network.

deployments. We assess the throughput of the two networks under these three different tag deployment scenarios.

We deployed 7 tags using two additional deployment methods. In these two alternative deployments, the tags are no longer uniformly distributed. We measured the overall throughput of the two networks under these two special deployments as well as the uniform deployment setting.

In the non-uniform tag deployment environment, there may be a high concentration of tags near some readers, resulting in dense tag deployments in some areas. This uneven deployment negatively affects the throughput of both networks. As shown in Fig. 13, in the two non-uniform deployment scenarios considered in the experimental setup, the throughput of the TDMA network decreases by 22% from 72Kbps (uniform deployment) to 56Kbps, while the throughput of Trident changes by 15%, decreasing from 228Kbps (uniform deployment) to 195Kbps. The performance gain of Trident over the TDMA network also increases from 3.18× to 3.48× and 3.42× in these scenarios. This experiment illustrates that Trident has greater robustness in dealing with non-uniform tag deployments.

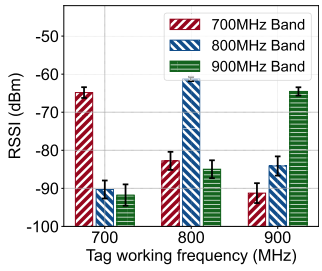

Fig. 14. The RSSI of tag signals when tags operating at various frequencies are excited by different excitation frequency bands.

C. Ablation Study

1) Frequency Selectivity of Reflector: We set the reader's frequencies to 700MHz, 800MHz, and 900MHz. And we set the operating frequency bands of the tag to the three aforementioned bands, respectively. The tag is placed at a distance of 70cm from the reader. We evaluate the strength of the backscattered signal received by the reader in different bands and use their difference to characterize the frequency selectivity of the reflector.

The results are depicted in Fig. 14. We observe that when the tag backscatter incident signals across multiple frequency bands, the backscattered signal received by the reader in the tag's operating frequency band is much stronger than the signal strength outside the reflector's operating frequency band. Specifically, when the reflector is set to 700MHz, the reader receives an excitation signal at -64.8dBm at the 700MHz band, whereas the excitation signals received in the 800MHz and 900MHz bands are only -82.8dBm and -91.3dBm, respectively. The difference in signal strength between the within-band and out-of-band signals exceeds 18dB. Therefore, we can conclude that the reflector can perform reflection at a single frequency band without affecting other frequency bands, demonstrating good frequency selectivity.

2) Accuracy of Band Detection: We assess the accuracy of frequency band detection in environments with two and three frequency bands of excitation signals respectively. We place the Trident tag at an arbitrary position and record its band detection result. Then another USRP N210 is used to measure the RSSI of the excitation signals of various frequency bands at the tag's deployment point. We measure the accuracy of the

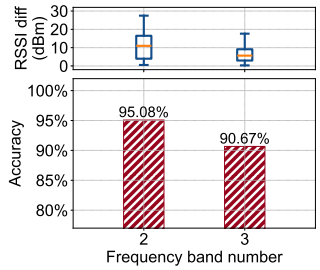

Fig. 15. The accuracy of detecting the strongest frequency component when a tag is excited by signals from multiple frequency bands.

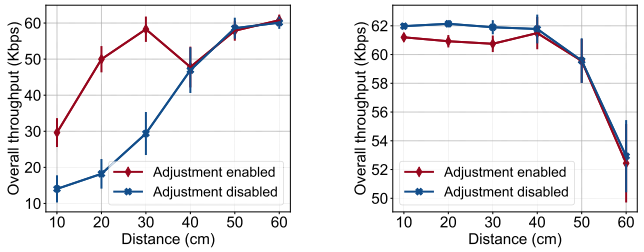

(a) The throughput of the interfered tags.

(b) The throughput of the interfering tags.

Fig. 16. Throughput comparison of tags with & w/o power adjustment in different distance settings between interfering tag and readers.

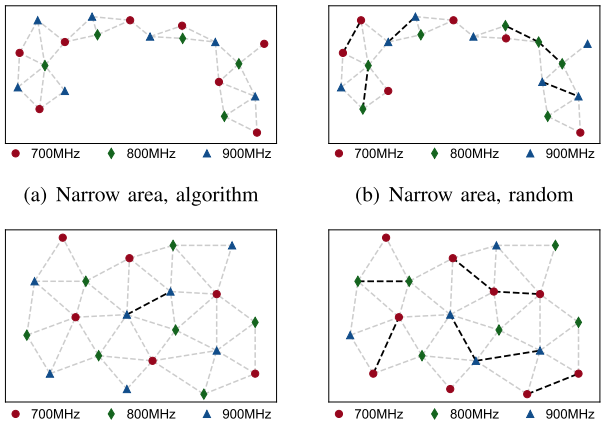

(a) Narrow area, algorithm

(b) Narrow area, random

(c) Wide area, algorithm

(d) Wide area, random

Fig. 17. Interference graph and frequency assignment of our algorithm and random selection in simulation. Each point in the graph represents a reader, and each dark edge indicates potential interference.

frequency band detector in selecting the strongest frequency band of the excitation signal. We conduct 80 experiments under the conditions of having two and three excitation frequency bands respectively.

The results are shown in Fig. 15. When there are two different frequency bands for excitation signals, the median RSSI difference between the two bands is 10.9dB. The band detection of Trident achieves an accuracy of 95.08% in detecting the strongest excitation frequency band. In the case of three frequency bands for excitation signals, the median RSSI difference between the strongest and second strongest bands is 5.6dB, and the band detection of Trident also achieves an accuracy of 90.67% in detecting the strongest excitation frequency band. This evaluation illustrates that in the majority of deployment locations, the frequency band detector can identify the frequency band with the strongest excitation signal with high accuracy.

3) Throughput Increment by Adjusting Reflection Power: We deploy two readers, R_A and R_B, at a distance of 3 meters and assign them to transmit excitation signals at the same frequency band. We deploy a tag T_α as an interfered tag at a distance of 50cm from R_A and another tag T_β as an interfering tag near R_B. We vary the distance D between T_β and R_B, and measure the throughput of both tags with reflection power adjuster enabled and disabled for the interfering tag.

The results are shown in Fig. 16. As the distance between T_β and R_B decreases, the throughput of the interfered R_A significantly decreases due to interference. As the interfering tag becomes closer to the reader, the throughput of T_α continues decreasing if the adjuster is disabled. Especially when D decreases to 10cm, the throughput of T_α is only 14.1Kbps. On the other hand, if the reflection power adjuster is enabled, the interfering T_β with the reflection power adjuster detects excessive excitation signals and actively adjusts the reflection strength when D is less than 32cm. As a result, the throughput of the interfered T_α increases to 58.3Kbps when D is 30cm, and it can maintain a throughput of 29.6Kbps (2.1× enhancement) even when D decreases to 10cm.

Besides, the adaptive reflection power adjustment has minimal cost on the throughput of the tag T_β. When the distance D is less than 30cm and the reflection power decreases, the throughput of the tag only drops from 62.0Kbps to 60.8Kbps, indicating negligible throughput loss.

4) Solution Quality of Frequency Assignment Algorithm: We simulate wide and narrow deployment environments, each with 20 readers. We assign frequencies to the readers by the algorithm proposed in Sec.III. We set a baseline that uses the best method from 200,000 randomly generated strategies. We consider the number of adjacent reader pairs with the same frequency band as the measurement of the solution quality.

The interference graph and simulation results are depicted in Fig. 17. In the narrow deployment area, our algorithm discovered a frequency allocation strategy that completely avoids interference. In the wide deployment area, our algorithm identifies a frequency assignment with only 1 pair of readers potentially causing interference. However, the baseline method exhibits more than 5 pairs of adjacent readers with the same bands and causes more severe interference.

5) Interference Strength in Dynamic Channel: To further verify the performance of the algorithm in a dynamic fading wireless environment, we use a Markov stochastic process to model the fading of the wireless channel between readers [33]. We ran both the pre-assigning method and our frequency allocation algorithm with the reallocation mechanism in this environment, simulating the co-channel interference strength at each moment for both methods.

We record the co-frequency interference strength at 10,000 simulation moments, plotting an example of the interference strength over time and the CDF of the co-frequency interference strength in Fig. 18. We found that the median interference

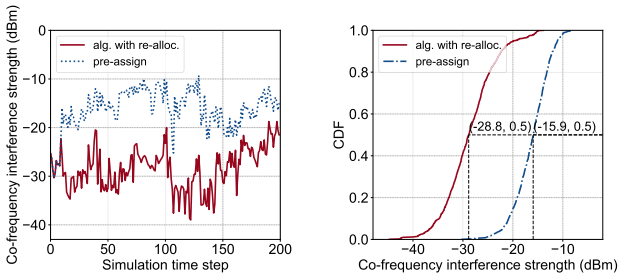

(a) An example of the interference strength over time (b) CDF of the interference strength

Fig. 18. Co-frequency interference strength of our algorithm and the pre-assigning method in the dynamic channel.

strength of our algorithm in the simulation is 55.3% of that of the pre-assigned method. This is because the pre-assigned method cannot adapt to the changing channel fading, whereas our algorithm can adopt new strategies when the channel environment changes significantly.

VII. Related Work

Due to the highly restricted energy consumption, backscatter tags cannot utilize the coordination schemes typically applied in traditional communication systems to mitigate interference. To address the issue, solutions have been proposed from two perspectives: interference avoidance and parallel decoding.

A. Interference Avoidance

The core of interference avoidance is to coordinate the signals onto orthogonal dimensions, utilizing the orthogonality to avoid interference [34], [35]. Typically, the orthogonal spatial dimensions used by researchers include the time domain, frequency domain, code domain, and spatial domain.

There are many existing works on utilizing the time domain for interference avoidance in the multi-reader network. These methods usually coordinate the tags backscatter at a desired time [13], [14], [16], [36], [37], [38], [39]. In [13] and [14], the reader runs a distributed slot reservation protocol, excites tags only in reserved time slots. Reference [16] proposes a scheme where the reader listens to channels before exciting the tag. It will back off when it detects that another reader is working. In [15], [36], and [37], the readers are controlled by a server, which schedules the readers' working slots. Some methods use multiple channels to provide more bandwidth. However, the critical problem in the multi-reader network is how to utilize the bandwidth resources. And these methods based on simple frequency division can't use the bandwidth resources effectively to avoid the interference, unless the tags are frequency-selective [40].

In single-reader scenarios, some approaches point out that the frequency domain can be also utilized for backscatter tags' coordination [27], [41], [42]. Especially, methods proposed in [27], [41] enable the OFDMA backscatter system by utilizing the frequency shifting on tags, which achieves interference avoidance in the single-reader network. However, in the multi-reader network, these methods can't adapt to the backscatter network topology changes caused by the dynamic wireless channel, and the tags are still possible to interfere with the adjacent readers. Besides, the frequency shifting requires a high-frequency clock or VCO, which causes more power consumption [27], [29].

There have also been efforts exploring backscatter coordination in the spatial domain and code domain [43], [44], [45]. [43] proposed a CDMA backscatter system by using different pseudo-noise (PN) codes on tags to spread their information. Reference [45] suggests utilizing narrow beams of the millimeter-wave to spatially coordinate backscattered signals, thus avoiding interference. Reference [30] further utilizes the beamforming mechanism of commercial mmWave Wi-Fi to achieve interference avoidance. [46] utilizes the leaky wave antennas (LWA), to avoid interference through frequency-space division in the above-100GHz frequency band. Different from these works, Trident proposes a novel interference avoidance scheme based on frequency-space division in multi-reader environments.

B. Parallel Decoding

Parallel decoding is a class of schemes that directly demodulate the information from interfered or collided signals to extract the tag's information. In [9], [47], [48], [49], and [50], parallel decoding algorithms are proposed. These methods utilize the symbol clusters on constellation diagrams caused by collided signals, to directly demodulate the information from collided signals. Specifically, these methods can handle small-scale collisions (e.g. the single-reader scenario). But in a multi-reader setting, a reader can be interfered with by tags excited by many adjacent readers. Under such complex interference, the communication and computation expense of these methods will significantly increase and eventually become unaffordable. While Trident utilizes the tag's frequency selectivity to avoid interference at a very low cost.

Researchers also notice the sparsity of the FFT spectrum after dechirping LoRa chirps. They have proposed parallel demodulation algorithms that can handle up to 256 LoRa backscattered signals [28], [29], [51]. By exploring the characteristic that the farther a tag is from the reader, the lower its reflected energy, [52] utilizes power-domain Non-Orthogonal Multiple Access (NOMA) technology and receives messages from multiple tags.

VIII. Conclusion

We present the design, implementation, and evaluation of Trident, a novel tag design to enable interference avoidance based on frequency-space division. The tag detects channel conditions and adaptively adjusts the frequency band and power of backscattered signals. We also propose an algorithm, assigning the adjacent readers to operate at different bands. With these designs, the Trident network avoids interference while maintaining high overall throughput by utilizing both the frequency and space domain. The results demonstrate that Trident enhances the network throughput by 3.18×, compared to the TDMA-based scheme.

REFERENCES

[1] X. Na, X. Guo, Z. Yu, J. Zhang, Y. He, and Y. Liu, "Leggiero: Analog WiFi backscatter with payload transparency," in *Proc. MobiSys*, 2023, pp. 436–449.

[2] V. Talla, M. Hessar, B. Kellogg, A. Najafi, J. R. Smith, and S. Gollakota, "LoRa backscatter: Enabling the vision of ubiquitous connectivity," *ACM Interact., Mobile, Wearable Ubiquitous Technol.*, vol. 1, no. 3, pp. 1–24, 2017.

[3] Y. Sun, W. Wang, L. Mottola, R. Wang, and Y. He, "BIFROST: Reinventing WiFi signals based on dispersion effect for accurate indoor localization," in *Proc. ACM SenSys*, 2023, pp. 376–389.

[4] Z. Chi, X. Liu, W. Wang, Y. Yao, and T. Zhu, "Leveraging ambient LTE traffic for ubiquitous passive communication," in *Proc. ACM SIGCOMM*, 2020, pp. 172–185.

[5] D. Bharadia, K. R. Joshi, M. Kotaru, and S. Katti, "BackFi: High throughput WiFi backscatter," *ACM SIGCOMM Comput. Commun. Rev.*, vol. 45, no. 4, pp. 283–296, Sep. 2015.

[6] A. Y. Majid, M. Jansen, G. O. Delgado, K. S. Yildirim, and P. Pawellzak, "Multi-hop backscatter tag-to-tag networks," in *Proc. IEEE INFOCOM*, 2019, pp. 721–729.

[7] B. Kellogg, V. Talla, S. Gollakota, and J. R. Smith, "Passive Wi-Fi: Bringing low power to Wi-Fi transmissions," in *Proc. USENIX NSDI*, 2016, pp. 151–164.

[8] A. Abedi, F. Dehbashi, M. H. Mazaheri, O. Abari, and T. Brecht, "WiTAG: Seamless WiFi backscatter communication," in *Proc. ACM SIGCOMM*, Jul. 2020, pp. 240–252.

[9] X. Guo et al., "Aloba: Rethinking ON-OFF keying modulation for ambient LoRa backscatter," in *Proc. ACM SenSys*, 2020, pp. 192–204.

[10] P. Zhang, M. Rostami, P. Hu, and D. Ganesan, "Enabling practical backscatter communication for on-body sensors," in *Proc. ACM SIGCOMM*, 2016, pp. 370–383.

[11] R. Mohammad, S. Karthik, C. Eugene, R. Sampath, and G. Deepak, "Redefining passive in backscattering with commodity devices," in *Proc. ACM MobiCom*, 2020, pp. 1–13.

[12] A. Bletsas, S. Siachalou, and J. Sahalos, "Anti-collision backscatter sensor networks," *IEEE Trans. Wireless Commun.*, vol. 8, no. 10, pp. 5018–5029, Oct. 2009.

[13] J. Waldrop, D. W. Engels, and S. E. Sarma, "Colorwave: An anticollision algorithm for the reader collision problem," in *Proc. IEEE ICC*, May 2003, pp. 1206–1210.

[14] F. Gandino, R. Ferrero, B. Montrucchio, and M. Rebaudengo, "Increasing throughput in RFID multi-reader environments avoiding reader-to-reader collisions," in *Proc. IEEE ICCE*, Jan. 2011, pp. 37–38.

[15] Z. Zhou, H. Gupta, S. R. Das, and X. Zhu, "Slotted scheduled tag access in multi-reader RFID systems," in *Proc. IEEE ICNP*, Oct. 2007, pp. 61–70.

[16] S. M. Birari and S. Iyer, "Mitigating the reader collision problem in RFID networks with mobile readers," in *Proc. IEEE ICON*, Nov. 2005, pp. 1–6.

[17] F. Dehbashi, A. Abedi, T. Brecht, and O. Abari, "Verification: Can WiFi backscatter replace RFID?" in *Proc. ACM MobiCom*, 2021, pp. 97–107.

[18] I. C. Hunter and J. D. Rhodes, "Electronically tunable microwave bandpass filters," *IEEE Trans. Microw. Theory Techn.*, vol. MMT-30, no. 9, pp. 1354–1360, Sep. 1982.

[19] TOSHIBA. *1sv285 Datasheet*. Accessed: Nov. 11, 2024. [Online]. Available: toshiba.semicon-storage.com/ap-en/semiconductor/product/diodes/detail.1SV285.html

[20] NXP. *Bb145 Datasheet*. Accessed: Nov. 11, 2024. [Online]. Available: www.nxp.com/part/BB145B#/

[21] J. D. Griffin and G. D. Durgin, "Complete link budgets for backscatter-radio and RFID systems," *IEEE Antennas Propag. Mag.*, vol. 51, no. 2, pp. 11–25, Apr. 2009.

[22] A. D. Cooperation. *Lt5534 Datasheet*. Accessed: Nov. 11, 2024. [Online]. Available: www.analog.com/en/products/lt5534.html

[23] T. D. Novlan, R. K. Ganti, A. Ghosh, and J. G. Andrews, "Analytical evaluation of fractional frequency reuse for OFDMA cellular networks," *IEEE Trans. Wireless Commun.*, vol. 10, no. 12, pp. 4294–4305, Dec. 2011.

[24] X. Guo et al., "Saiyan: Design and implementation of a low-power demodulator for LoRa backscatter systems," in *Proc. USENIX NSDI*, 2022, pp. 437–451.

[25] S. Li et al., "Passive DSSS: Empowering the downlink communication for backscatter systems," in *Proc. USENIX NSDI*, 2022, pp. 913–928.

[26] P. Zhang, D. Bharadia, K. Joshi, and S. Katti, "HitchHike: Practical backscatter using commodity WiFi," in *Proc. SenSys*, 2016, pp. 259–271.

[27] R. Zhao et al., "OFDMA-enabled Wi-Fi backscatter," in *Proc. MobiCom*, 2019, pp. 1–15.

[28] M. Hessar, A. Najafi, and S. Gollakota, "NetScatter: Enabling large-scale backscatter networks," in *Proc. USENIX NSDI*, 2019, pp. 271–284.

[29] J. Jiang, Z. Xu, F. Dang, and J. Wang, "Long-range ambient LoRa backscatter with parallel decoding," in *Proc. ACM MobiCom*, 2021, pp. 684–696.

[30] Y. Chae, Z. Lin, K. M. Bae, S. Kim, and P. Pathak, "mmComb: High-speed mmWave commodity WiFi backscatter," in *Proc. USENIX NSDI*, 2024, pp. 1713–1729.

[31] M. Dunna, M. Meng, P.-H. Wang, C. Zhang, P. Mercier, and D. Bharadia, "SyncScatter: Enabling WiFi like synchronization and range for WiFi backscatter communication," in *Proc. USENIX NSDI*, 2021, pp. 923–937.

[32] B. A. Sharp, E. A. Grindrod, and D. A. Camm, "Hybrid TDMA/CSMA protocol for self managing packet radio networks," in *Proc. IEEE ICUPC*, Nov. 1995, pp. 929–933.

[33] A. Seetharam, J. Kurose, D. Goeckel, and G. Bhanage, "A Markov chain model for coarse timescale channel variation in an 802.16e wireless network," in *Proc. IEEE INFOCOM*, Mar. 2012, pp. 1800–1807.

[34] W. Wang et al., "MicNest: Long-range instant acoustic localization of drones in precise landing," in *Proc. ACM SenSys*, 2022, pp. 504–517.

[35] Y. He et al., "Acoustic localization system for precise drone landing," *IEEE Trans. Mobile Comput.*, vol. 23, no. 5, pp. 4126–4144, May 2024.

[36] M. Katanbaf, A. Saffari, and J. R. Smith, "MultiScatter: Multistatic backscatter networking for battery-free sensors," in *Proc. ACM Sensys*, 2021, pp. 69–83.

[37] D. F. Perez-Ramirez, C. Pérez-Penichet, N. Tsiftes, T. Voigt, D. Kostić, and M. Boman, "DeepGANTT: A scalable deep learning scheduler for backscatter networks," in *Proc. ACM IPSN*, 2023, pp. 163–176.

[38] P. Zhang, C. Josephson, D. Bharadia, and S. Katti, "FreeRider: Backscatter communication using commodity radios," in *Proc. ACM CoNEXT*, 2017, pp. 389–401.

[39] W. Liu, K. Huang, X. Zhou, and S. Durrani, "Full-duplex backscatter interference networks based on time-hopping spread spectrum," *IEEE Trans. Wireless Commun.*, vol. 16, no. 7, pp. 4361–4377, Jul. 2017.

[40] R. Alesii, P. D. Marco, F. Santucci, P. Savazzi, R. Valentini, and A. Vizziello, "Multi-reader multi-tag architecture for UWB/UHF radio frequency identification systems," in *Proc. Int. EURASIP Workshop RFID Technol. (EURFID)*, Oct. 2015, pp. 28–35.

[41] F. Zhu, Y. Feng, Q. Li, X. Tian, and X. Wang, "DigiScatter: Efficiently prototyping large-scale OFDMA backscatter networks," in *Proc. ACM MobiSys*, 2020, pp. 42–53.

[42] J. Mitsugi, Y. Kawakita, K. Egawa, and H. Ichikawa, "Perfectly synchronized streaming from digitally modulated multiple backscatter sensor tags," in *Proc. IEEE RFID-TA*, 2018, pp. 1–6.

[43] N. Mi et al., "CBMA: Coded-backscatter multiple access," in *Proc. IEEE ICDCS*, Jul. 2019, pp. 799–809.

[44] C. Mutti and C. Floerkemeier, "CDMA-based RFID systems in dense scenarios: Concepts and challenges," in *Proc. IEEE RFID*, Apr. 2008, pp. 215–222.

[45] M. H. Mazaheri, A. Chen, and O. Abari, "MmTag: A millimeter wave backscatter network," in *Proc. ACM SIGCOMM*, Aug. 2021, pp. 463–474.

[46] A. Kludze and Y. Ghasempour, "LeakyScatter: A frequency-agile directional backscatter network above 100 GHz," in *Proc. USENIX NSDI*, 2023, pp. 375–388.

[47] M. Jin, Y. He, X. Meng, Y. Zheng, D. Fang, and X. Chen, "FlipTracer: Practical parallel decoding for backscatter communication," in *Proc. ACM MobiCom*, 2017, pp. 275–287.

[48] P. Hu, P. Zhang, and D. Ganesan, "Laissez-faire: Fully asymmetric backscatter communication," *ACM SIGCOMM Comput. Commun. Rev.*, vol. 45, no. 4, pp. 255–267, Sep. 2015.

[49] M. Jin, Y. He, X. Meng, D. Fang, and X. Chen, "Parallel backscatter in the wild: When burstiness and randomness play with you," in *Proc. ACM MobiCom*, 2018, pp. 471–485.
[50] J. Ou, M. Li, and Y. Zheng, "Come and be served: Parallel decoding for COTS RFID tags," in *Proc. ACM MobiCom*, 2015, pp. 500–511.
[51] Y. Peng et al., "PLoRa: A passive long-range data network from ambient LoRa transmissions," in *Proc. ACM SIGCOMM*, Aug. 2018, pp. 147–160.
[52] J. Guo, X. Zhou, S. Durrani, and H. Yanikomeroglu, "Design of non-orthogonal multiple access enhanced backscatter communication," *IEEE Trans. Wireless Commun.*, vol. 17, no. 10, pp. 6837–6852, Oct. 2018.

Yang Zou (Student Member, IEEE) received the B.E. degree from Beijing University of Aeronautics and Astronautics (BUAA). He is currently pursuing the Ph.D. degree with Tsinghua University. His research interests include wireless networking and communication.

Xin Na (Student Member, IEEE) received the B.E. degree from Tsinghua University, Beijing, China, where he is currently pursuing the Ph.D. degree. His research interests include wireless networking and low-power IoT.

Yimiao Sun (Student Member, IEEE) received the B.E. degree from the University of Electronic Science and Technology of China (UESTC). He is currently pursuing the Ph.D. degree with Tsinghua University. His research interests include mobile computing and wireless sensing.

Yuan He (Senior Member, IEEE) received the B.E. degree from the University of Science and Technology of China, the M.E. degree from the Institute of Software, Chinese Academy of Sciences, and the Ph.D. degree from The Hong Kong University of Science and Technology. He is currently an Associate Professor with the School of Software and BNRist, Tsinghua University. His research interests include wireless networks, the Internet of Things, pervasive, and mobile computing. He is a member of ACM.